

PAPER • OPEN ACCESS

## Non-thermal alloyed ohmic contact process of GaN-based HEMTs by pulsed laser annealing

To cite this article: An-Jye Tzou *et al* 2016 *Semicond. Sci. Technol.* **31** 055003

View the [article online](#) for updates and enhancements.

You may also like

- [High-Quality AlGaIn/GaN HEMTs Growth on Silicon Using Al<sub>0.55</sub>Ga<sub>0.45</sub>N as Interlayer for High RF Applications](#)  
Tsu-Ting Lee, Le Trung Hieu, Chung-Han Chiang *et al.*
- [Immune-stealth VP28-conjugated heparin nanoparticles for enhanced and reversible anticoagulation](#)  
Hussein Reda Hussein, Chia-Yu Chang, Yini Zheng *et al.*
- [Low-hole concentration polycrystalline germanium by CO<sub>2</sub> laser annealing for the fabrication of an enhancement-mode nMOSFET](#)  
Hari Anand Kasirajan, Wen-Hsien Huang, Ming-Hsuan Kao *et al.*



**ECS**  
The  
Electrochemical  
Society  
Advancing solid state &  
electrochemical science & technology

**DISCOVER**  
how sustainability  
intersects with  
electrochemistry & solid  
state science research

# Non-thermal alloyed ohmic contact process of GaN-based HEMTs by pulsed laser annealing

An-Jye Tzou<sup>1,2</sup>, Dan-Hua Hsieh<sup>2</sup>, Szu-Hung Chen<sup>3</sup>, Zhen-Yu Li<sup>4</sup>,  
Chun-Yen Chang<sup>1,5,6</sup> and Hao-Chung Kuo<sup>2,3</sup>

<sup>1</sup> Department of Electrophysics, National Chiao Tung University, 1001 Ta Hsueh Road, Hsinchu 30010, Taiwan

<sup>2</sup> Department of Photonics and Institute of Electro-Optical Engineering, National Chiao Tung University, Hsinchu 30010, 1001 Ta Hsueh Road, Hsinchu 30010, Taiwan

<sup>3</sup> National Nano Device Laboratories, No.26, Prosperity Road 1, Hsinchu 30078, Taiwan

<sup>4</sup> Epistar, 22 Keya Road, Daya, Central Taiwan Science Park, Taichung 42881, Taiwan

<sup>5</sup> Department of Electronics Engineering, National Chiao Tung University, 1001 Ta Hsueh Road, Hsinchu 30010, Taiwan

<sup>6</sup> Research Center for Applied Sciences, Academia Sinica, 128 Academia Road, section 2, Nankang, Taipei 11529, Taiwan

E-mail: [hckuo@faculty.nctu.edu.tw](mailto:hckuo@faculty.nctu.edu.tw)

Received 11 October 2015, revised 10 February 2016

Accepted for publication 11 February 2016

Published 15 March 2016



CrossMark

## Abstract

We have demonstrated Si implantation incorporation into GaN HEMTs with a non-alloyed ohmic contact process. We optimized the power density of pulsed laser annealing to activate implanted Si dopants without a thermal metallization process. The experimental results show that the GaN surface will be reformed under the high power density of the illumination conditions. It provides a smooth surface for following contact engineering and leads to comparable contact resistance. The transmission line model (TLM) measurement shows a lower contact resistance to  $6.8 \times 10^{-7} \Omega \cdot \text{cm}^2$  via non-alloyed contact technology with significantly improved surface morphology of the contact metals. DC measurement of HEMTs shows better current and on-resistance. The on-resistance could be decreased from 2.18 to 1.74  $\text{m}\Omega\text{-cm}^2$  as we produce a lower contact resistance. Pulsed laser annealing also results in lower gate leakage and smaller dispersion under a pulse  $I$ - $V$  measurement, which implies that the density of the surface state is improved.

Keywords: GaN, HEMTs, pulse laser annealing, ion implantation

(Some figures may appear in colour only in the online journal)

## 1. Introduction

GaN-based high electron mobility transistors (HEMTs) attract a lot of interest due to their high electric breakdown field and higher sheet carrier density ( $n_s$ ) of two-dimensional electron

gas (2DEG), promising a superior breakdown voltage ( $V_B$ ) and lower on-state resistance ( $R_{\text{on}}$ ) for the applications in DC/DC convertors or DC/AC inverters [1]. For high power electronic device applications, it is essential to improve the contact resistance so that  $R_{\text{on}}$  could be diminished [2]. In general, stacking metal with thermal metallization under a nitrogen atmosphere is widely used to serve as an ohmic contact process for GaN-based HEMTs, and shows a specific contact resistance ( $\rho_s$ ) of about  $8 \times 10^{-6} \Omega \cdot \text{cm}^2$  [3]. However, it has been reported that deep alloy spikes are formed



Original content from this work may be used under the terms of the Creative Commons Attribution 3.0 licence. Any further distribution of this work must maintain attribution to the author(s) and the title of the work, journal citation and DOI.

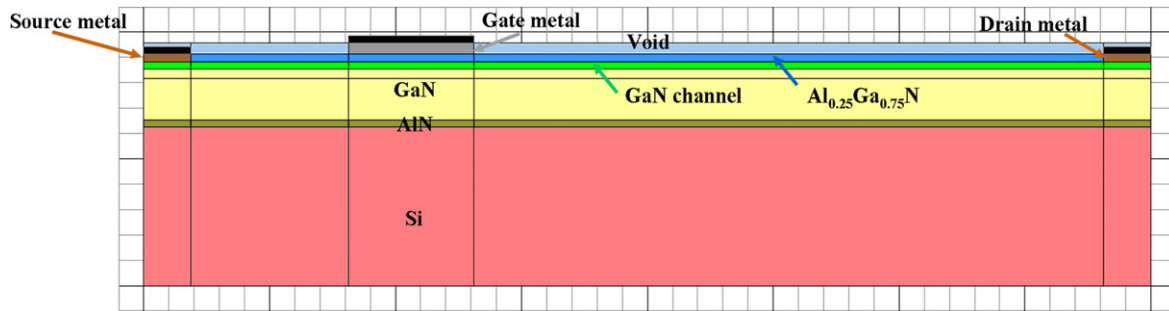


**Figure 1.** Schematic diagram of the GaN HEMT structure for our simulations.

under ohmic contact metal regions due to the thermal metallization process [4], which results in leakage to the buffer layer structures due to an unexpected electric field at the sharp points of the spikes [5]. Furthermore, high temperature thermal metallization performed at 800 °C or higher is responsible for a rough morphology. The rough surface morphology reduces the tolerance of subsequent lithography alignment, especially for a hard contact type aligner [6]. Hence, it is necessary to develop a non-alloyed process with a comparable contact resistance for GaN-based HEMTs.

Some demonstrations of ion implantation into source/drain (S/D) regions for a non-alloyed ohmic contacts process have been reported [6–8]. Comparable contact resistance was obtained due to the implanted *n*-GaN reducing the barrier height of the metal-semiconductor interface [6–8]. Ion implantation for selective doping is widely used for the Si-based integrated circuits (ICs) industry. However, implantation into GaN-based devices has been a challenging task due to their refractory nature as well as GaN needing to be grown at high temperature with high nitrogen vapor pressure [6, 9]. The thermal activation of implanted dopants and the damage recovery of implanted GaN regions require annealing at temperatures above 1500 °C with a nitrogen atmosphere pressure more than 15 kbar at equilibrium [10], which is difficult to apply advantageously to the manufacture of normal ICs. Furthermore, high temperature annealing will lead to Ga dissociation from the GaN surface, resulting in a rough surface and also breaking the interface between AlGa<sub>0.25</sub>N and GaN, hence the sheet concentration of 2DEG will be reduced [11, 12].

In this work, we use Si-implantation herein the unintentionally doped GaN for S/D regions with the purpose to obtain low specific contact resistance without a thermal alloy process. However, we need to avoid thermal damage of the AlGa<sub>0.25</sub>N/GaN interface when we activate the implanted dopants. Therefore, pulsed laser annealing was employed to activate implanted Si dopants instead of rapid thermal annealing (RTA). The surface damage from laser exposure will be suppressed due to the transient interaction as the pulse laser beam exposes the GaN surface, but the high power laser probing provides enough thermal energy to activate the dopants. In the meantime, the AlN capping layer is capped as a sacrificed mask to prevent dissociation of GaN under an exposed high power density laser, therefore a smooth surface

will be retained and the 2DEG sheet concentration remains. The non-alloyed S/D metal contact shows lower contact resistance and the device performance could be enhanced.

## 2. Device modelling

Firstly, a two-dimensional simulation was employed to determine the doping concentration of ion-implanted *n*-GaN for S/D regions. The reference sample in this paper is called reference HEMT without Si-implantation into S/D regions. In comparison to the reference sample, the Si-implanted S/D of GaN-based HEMT leads to a higher doping level for S/D regions. Based on our designs, the band structure and electrical properties of the Si-implanted HEMT is calculated by APSYS simulation software, which was developed by *Crosslight Software Inc.* The simulated structure of the GaN-based HEMT is shown in figure 1.

The stacking metal system, such as Ti/Al/Ni/Au multilayers were generally deposited on GaN to serve as an ohmic contact. The effective barrier at the interface is large due to the higher energy band gap of GaN, near 3.39 eV. Therefore, the Schottky barrier height is not low enough to yield a current transport without interruption. Lu *et al* have found that the TiN will be formed when Ti reacts with *n*-GaN [13]. A large amount of nitrogen vacancies ( $V_N$ ) will be produced near the interface between Ti and *n*-GaN after thermal alloying, which shows a sharp semiconductor band bending with a heavily-doped *n*-GaN. Lin *et al* also reported that the Fermi level will shift to the energy level of the nitrogen vacancy regarding Fermi level pinning at 0.5 eV below the edge of the conduction band [14]. The sharp band bending of *n*-GaN leads to electron tunnelling probability, hence the electrons are promising transport from *n*-GaN to Ti as free carriers. The experimental results consisted of theoretical calculations, which implied that the alloyed ohmic contact between Ti and *n*-GaN was attributed to electron tunnelling rather than reduction of the Schottky barrier height.

However, the ohmic contact via thermal alloying is not identical to our case. The barrier height ( $\phi_b$ ) between Ti and *n*-GaN without alloying could be calculated to be 0.2 eV by using equation (1), where the work function of Ti ( $\phi_m$ ) is 4.3 eV and the electron affinity of GaN ( $\chi$ ) is 4.1 eV,

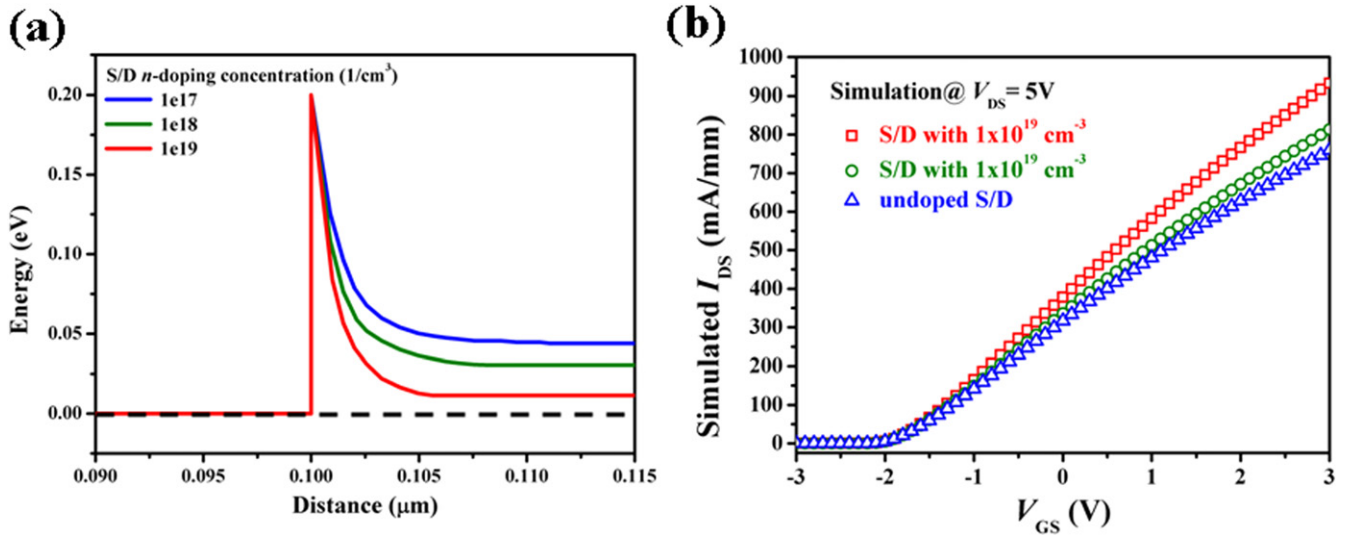


**Figure 2.** (a) The simulated band structure of the ohmic contact metal and  $n$ -GaN. (b) The simulated  $I_{DS}$ - $V_{GS}$  curves of HEMTs with different S/D doping concentration. The device has a  $2 \mu\text{m}$  gate length ( $L_G$ ), a  $4 \mu\text{m}$  source-to-gate distance ( $L_{SG}$ ), and a  $20 \mu\text{m}$  gate-to-drain distance ( $L_{GD}$ ).

respectively.

$$\phi_b = \phi_m - \chi \quad (1)$$

This means that the Schottky barrier height could not be modified according to the doping level of  $n$ -GaN. Although we understand that the mechanism of the ohmic contact for  $n$ -GaN is necessary to the doping level, it does in fact conflict with the experimental results. According to our simulation, heavily doped  $n$ -GaN with  $N_D$  of  $1 \times 10^{19} \text{cm}^{-3}$  exhibits sharp natural band bending, as shown in figure 2(a). As the doping level becomes heavier, the barrier near the interface became extremely thin but the barrier height remains  $0.2 \text{eV}$ , which is still lower than that of the thermal alloying ohmic contact [14]. The barrier of heavily doped  $n$ -GaN is thin enough and yields a flow of electrons via tunnelling, leading to lower contact resistance. The simulations imply that we could reach lower contact resistance by using this doping concentration of  $n$ -GaN.

Based on our simulated results, we also simulated the DC characteristics of HEMT w/ and w/o implantation into the S/D regions. The  $I_{DS}$ - $V_{GS}$  curves of the reference sample (w/o S/D implantation),  $1 \times 10^{18} \text{cm}^{-3}$ , and  $1 \times 10^{19} \text{cm}^{-3}$  of Si-doped  $n$ -GaN for S/D regions through ion implantation were discussed, respectively. As expected, the GaN-based HEMT with  $1 \times 10^{19} \text{cm}^{-3}$  of  $n$ -doping concentration for S/D regions shows an improved  $I_{DS}$  current, reaching  $763 \text{mA/mm}$  at  $V_{GS} = 2 \text{V}$ . The simulated  $I_{DS}$ - $V_{GS}$  curves were plotted in figure 2(b).

To obtain the  $1 \times 10^{19} \text{cm}^{-3}$  of S/D  $n$ -doping via Si implantation, the Transport of Ions in Matter (TRIM) simulation was carried out to determine the dose and angle for implanted Si dopants. The  $30 \text{keV}$  with  $20^\circ$  tilt,  $90 \text{keV}$  with  $0^\circ$  tilt, and  $190 \text{keV}$  with  $0^\circ$  tilt of Si-implantation was started, respectively. Figure 3 shows the TRIM simulation result, the depth profile of the Si-implanted dopants into the GaN layer

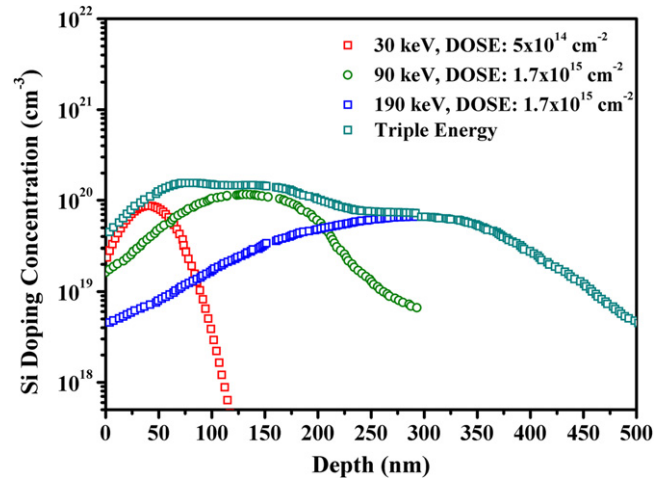


**Figure 3.** The simulated depth profiles of Si dopants in GaN layers. The implanted conditions were determined by TRIM simulation.

is investigated. The comparatively large tilt angle for  $30 \text{keV}$  implantation was a response to the ultra-high doping concentration ( $[\text{Si}] = 1 \times 10^{19} \text{cm}^{-3}$ ) in the surface of S/D, and leads to crucially low contact resistance without thermal metallization.

### 3. Experiment

The epitaxial structure of a HEMT was grown on a 6-inch Si substrate by using a metal-organic chemical vapor deposition (MOCVD) system. The epitaxy was started from a  $100 \text{nm}$ -thick AlN nucleation layer, followed by 100 periods of a carbon-doped AlN ( $4.5 \text{nm}$ -thick)/GaN ( $20 \text{nm}$ -thick) superlattices (SLs) buffer layer structure. Afterward, a  $1.6 \mu\text{m}$ -thick undoped GaN layer, and a  $20 \text{nm}$ -thick  $\text{Al}_{0.25}\text{Ga}_{0.75}\text{N}$  barrier

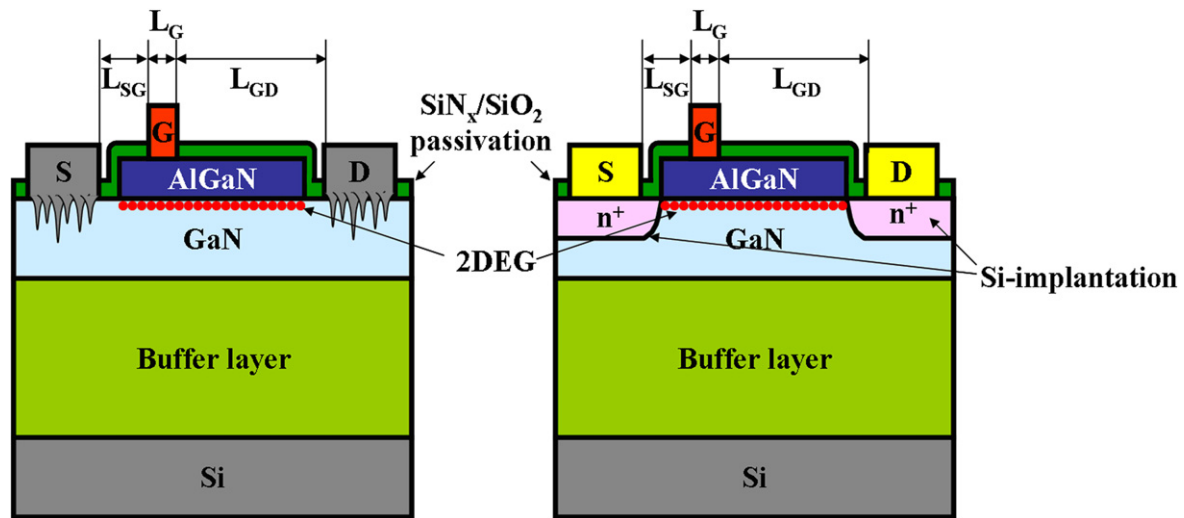


**Figure 4.** The cross-sectional diagram of AlGaIn/GaN HEMTs. The devices were fabricated w/ and w/o Si implantation into S/D regions, respectively.

layer with 2 nm GaN cap layer were grown on the superlattice structure.

The HEMT device process was started from mesa isolation by an inductivity coupled plasma reactive ion etching (ICP-RIE) system. Afterwards, the 20 nm-thick AlGaIn barrier layer was partially removed by a low etching rate ICP-RIE. The AlGaIn above the S/D regions was opened for the subsequent ion implantation. The following 20 nm-thick SiO<sub>2</sub> was deposited by plasma enhanced chemical vapor deposition (PECVD), to serve as the surface protection layer during ion-implantation. As mentioned above, the TRIM simulation determined the dose and energy of the implanted Si dopants. Afterwards, a SiO<sub>2</sub> protection layer was removed by BOE solution and a 20 nm-thick AlN capping layer was deposited by atomic layer deposition (ALD) at 650 °C. Subsequently, the laser annealing was employed to activate the Si dopants. A KrF excimer laser with a 248 nm line of wavelength, 20 ns of a pulse duration, and with energy density up to 2 J cm<sup>-2</sup> was used. The laser was condensed as a 5 × 5 mm<sup>2</sup> of spot size.

After the dopants activation by pulsed laser annealing, the AlN mask was removed by KOH solution. The SiN<sub>x</sub>/SiO<sub>2</sub> (20/280 nm) were grown for surface passivation and the stacking metal system of Ti/Al/Ni/Au (20 nm/120 nm/25 nm/100 nm) was subsequently evaporated on the S/D regions. After stacking metal deposition, a 850 °C/30 s thermal annealing by rapid thermal annealing (RTA) was employed to produce ohmic contact formation of the reference sample (w/o Si-implantation), but a non-thermal metallization for the Si-implanted sample was fabricated, respectively. Finally, the stacked Ni/Au (50 nm/300 nm) served as a Schottky gate. The device has a 2 μm gate length ( $L_G$ ), a 4 μm source-to-gate distance ( $L_{SG}$ ), and a 20 μm gate-to-drain distances ( $L_{GD}$ ). The schematic structure is shown in figure 4.

#### 4. Result and discussions

In the beginning of the device analysis, the power density of pulsed laser annealing was discussed. The most important part of this fabrication method is the activation process by pulsed laser annealing. The GaN layer can absorb the laser energy due to the energy band gap of GaN (3.4 eV) being smaller than the photon energy of the excimer laser with a wavelength of 248 nm (5 eV). The absorption coefficient ( $\alpha$ ) of GaN was  $2.1 \times 10^5 \text{ cm}^{-1}$  at the 248 nm [12], hence the absorption of GaN at 248 nm is extremely high but the AlN (6.2 eV) cap layer will not absorb the laser energy. Therefore, the AlN capping layer will not be damaged under that exposed by the laser and also retains compactness, so that the surface Ga dissociation will be suppressed by the AlN capping layer. By using this mechanism, the AlN capping layer plays an appropriate role for surface protection under 248 nm exposed by a laser.

In general, to activate the implanted Si dopants in GaN requires over 1500 °C at equilibrium [10]. When the pulsed laser illuminates the GaN surface, laser energy is first absorbed by GaN and most of the energy transfers into thermal energy. After that, the thermal conduction rapidly transmits heat to the exposed region so that the temperature increases abruptly. Therefore, the thermal energy from the laser beam will provide enough heat equivalent to activate the Si dopants. Meanwhile, due to the strong absorption of GaN from the 248 nm excimer laser, the high power density of the pulsed laser will reform the GaN surface regarding the localized melting. In this paper, we changed the incident power density from 1.0 to 2.0 J cm<sup>-2</sup> and the surface morphology can be observed by atomic force microscopy (AFM). The relationship of roughness to the effective energy density is depicted in figure 5. The root-mean-square (RMS) surface morphology was decreased from 3.7 to 1.2 nm. It is clear that pulsed laser annealing at a large power density will result in a

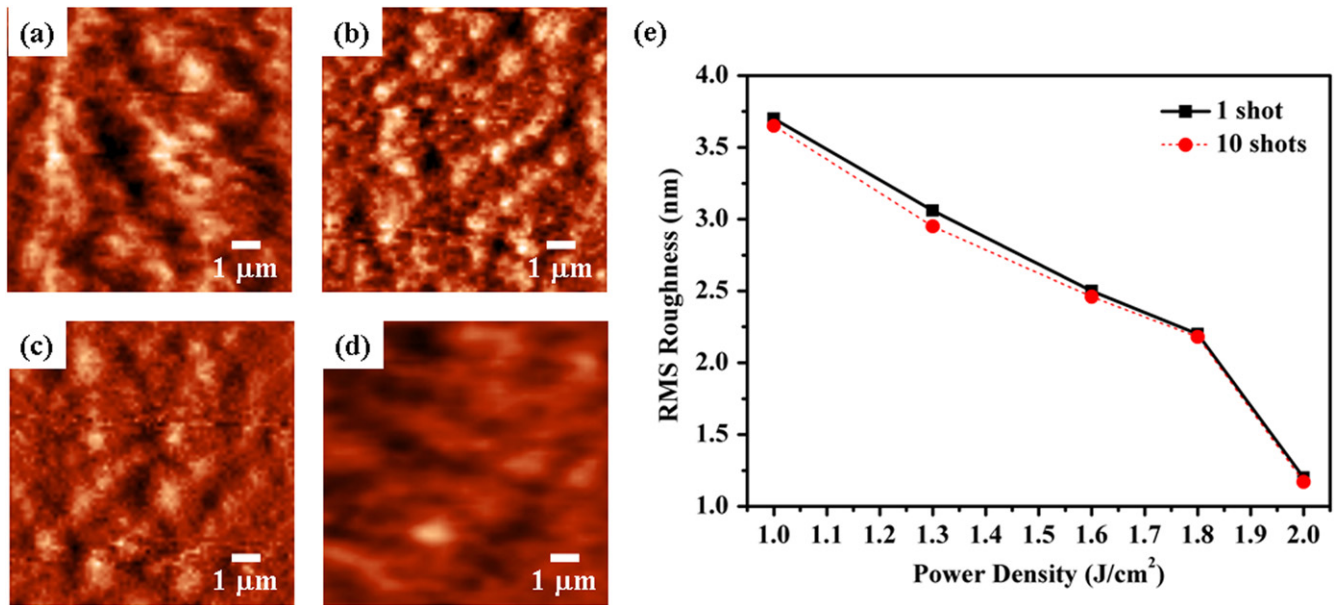


**Figure 5.** AFM surface morphology of (a) GaN surface after AlN was removed. The GaN surface after 10 shots of pulsed laser annealing with (b) 1.0, (c) 1.6, and (d) 2.0 J cm<sup>-2</sup> of power density, respectively. (e) RMS roughness of GaN surfaces with different incident power densities.

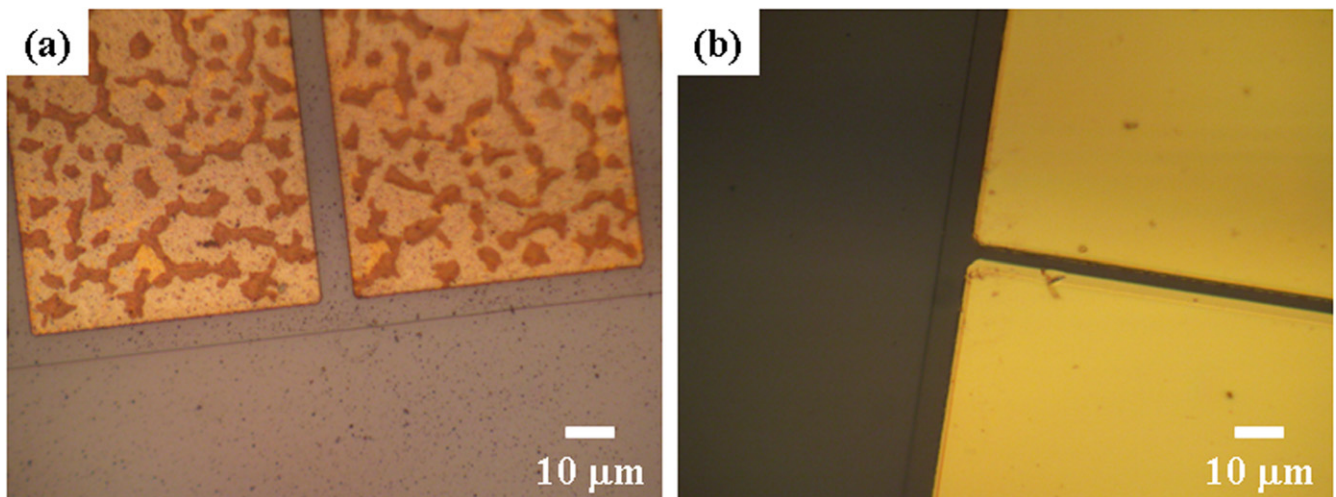


**Figure 6.** (a) Optical microscopy images of the Ti/Al/Ni/Au metal system for ohmic contact after alloying at 850 °C for 30 s. (b) As-deposited Ti/Al/Ni/Au metal system above the Si-implanted S/D regions.

reduction of RMS roughness. It is because a larger effective power density results in a larger molten depth, which leads to better melting of the GaN surface, also producing a smoother surface.

Ti/Al/Ni/Au (20 nm/120 nm/25 nm/100 nm) were grown on S/D regions by a lift-off process. For the reference sample (w/o implantation), ohmic contact was performed by thermal metallization at 850 °C, showing a rough surface after thermal annealing. The rough surface was due to the interdiffusion of ohmic contact metals, which result in bumpy surfaces after high temperature annealing [15, 16]. Due to heavily doped S/D regions by ion implantation, non-alloyed ohmic contact with excellent smooth surface morphology was realized. The metal surface morphologies with thermal metallization and with a non-alloyed process were shown in

figure 6, respectively. The transmission line model (TLM) measurement was employed to calculate the contact resistance. The reference sample shows  $2.2 \times 10^{-6} \Omega \cdot \text{cm}^2$  of contact resistance. Figure 7 shows the contact resistance with a different power density of pulse laser annealing. The TLM measurement results show that the contact resistance was reduced from  $3.8 \times 10^{-6}$  to  $6.8 \times 10^{-7} \Omega \cdot \text{cm}^2$  as we increased the power density of pulsed laser annealing. It means that the higher power density provides more thermal energy to activate further Si dopants in S/D regions, and that the contact resistance could be improved. Therefore, a high power density of pulsed laser annealing is necessary to improve the contact resistance and produces higher doping concentration of Si-implanted GaN. Simultaneously fabricated contacts on implanted areas without laser annealing

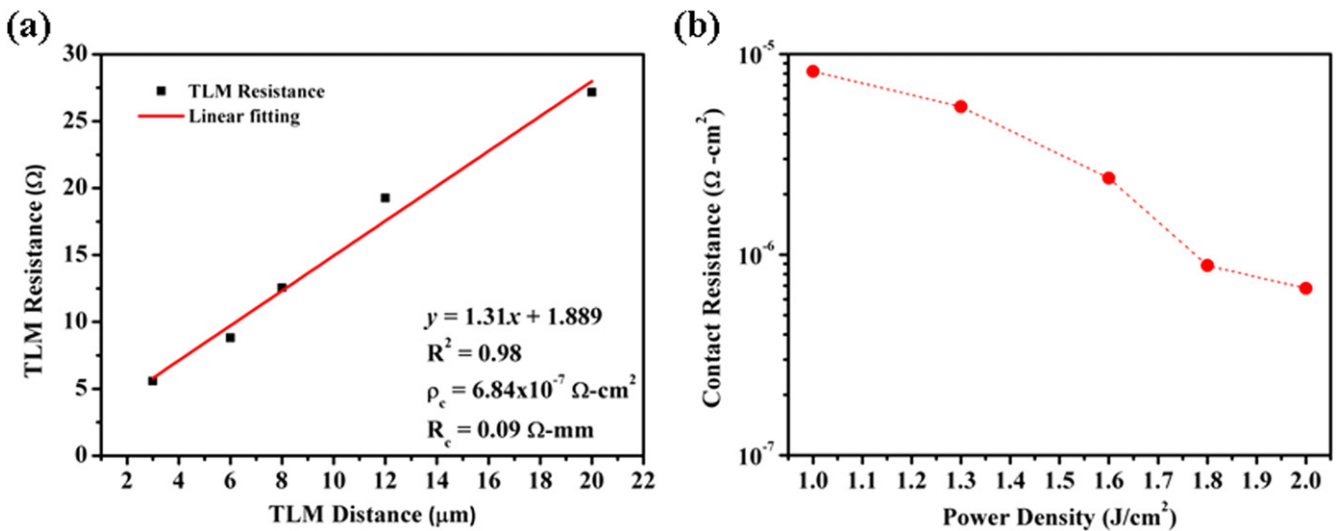


**Figure 7.** (a) The contact resistance calculation of the implanted sample with  $2.0 \text{ J cm}^{-2}$  pulsed laser annealing shows a low contact resistance. (b) The contact resistance with a different power density of pulsed laser annealing.

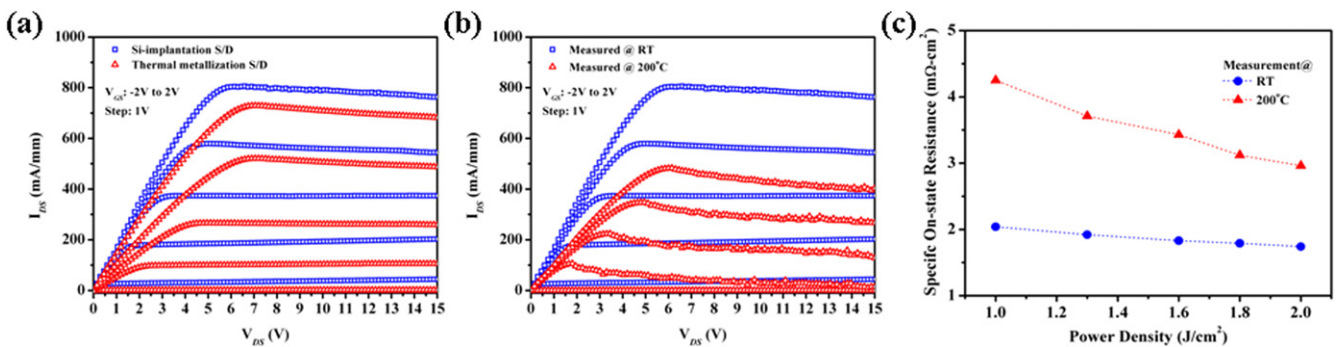


**Figure 8.** (a)  $I_{DS}$ - $V_{DS}$  curves of a Si-implanted S/D HEMT with  $2.0 \text{ J cm}^{-2}$  power density for pulsed laser annealing and the reference sample, respectively. (b) On-state  $I_{DS}$ - $V_{DS}$  characteristics of Si-implantation S/D HEMT with  $2.0 \text{ J cm}^{-2}$  pulsed laser annealing at room temperature and  $200^\circ\text{C}$ , respectively. (c) The on-state resistance versus power density of laser annealing at RT and  $200^\circ\text{C}$ , respectively.

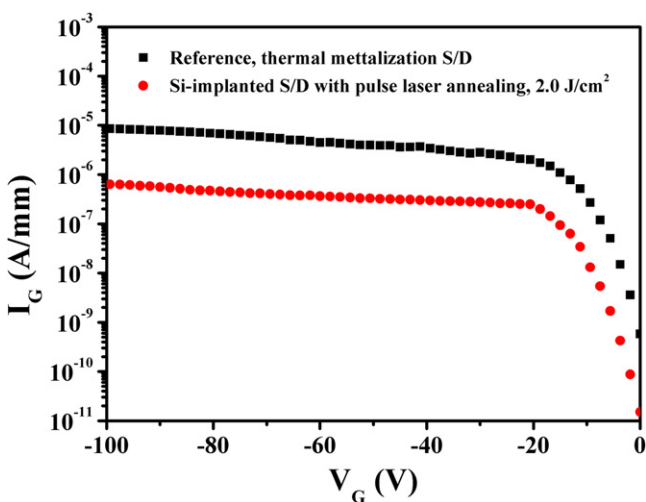


**Figure 9.** Reverse bias gate leakage currents of Schottky HEMTs w/ and w/o pulsed laser annealing,  $V_D = V_S = 0 \text{ V}$ .

show no ohmic contact, which implies that the activation of dopants exhibits the dominant mechanism of ohmic contact formation.

Figure 8(a) shows an  $I_{DS}$ - $V_{DS}$  comparison of the HEMTs between the reference sample and the Si-implanted S/D sample. The gate voltage was varied from  $-2 \text{ V}$  to  $2 \text{ V}$  in steps of  $1 \text{ V}$ . The  $I_{DS}$  of the Si-implanted S/D sample with  $2.0 \text{ J cm}^{-2}$  power density for pulsed laser annealing shows  $805 \text{ mA mm}^{-1}$  at  $V_{GS} = 2 \text{ V}$ , but only  $729 \text{ mA mm}^{-1}$  of  $I_{DS}$  was obtained from the reference sample. Derived from the results, the yielded specific on-state resistance ( $spec. R_{on}$ ) is  $1.74 \text{ m}\Omega\text{-cm}^2$  of the Si-implanted S/D HEMT, and  $2.18 \text{ m}\Omega\text{-cm}^2$  of the reference sample, respectively. The improved  $R_{on}$  implies that the Si-implantation into S/D regions with pulsed laser annealing is an excellent solution to achieve low contact resistance without thermal metallization. The following thermal stability under  $200^\circ\text{C}$  shows the good performance of Si-implanted S/D HEMTs. The on-state resistance was

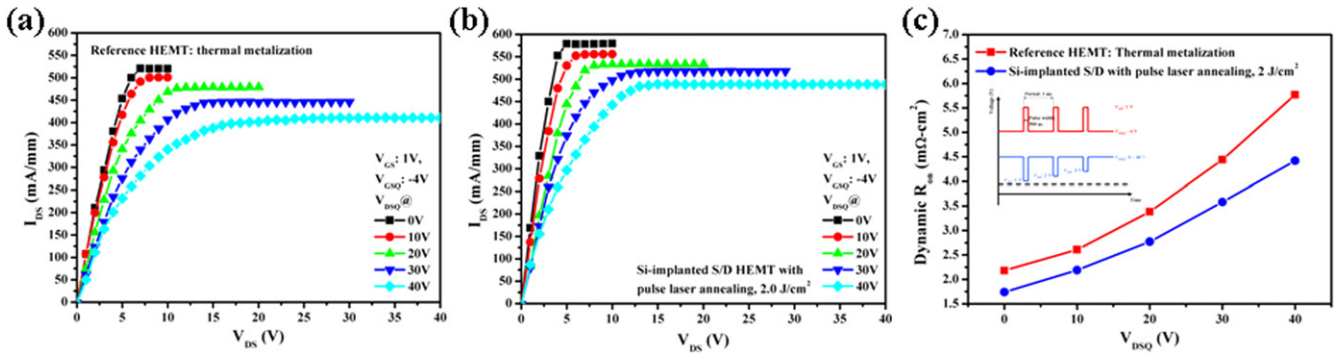


**Figure 10.** Pulsed  $I_{DS}$ - $V_{DS}$  characteristic of (a) the reference HEMT and (b) the Si-implantation S/D HEMT with  $2.0 \text{ J cm}^{-2}$  pulsed laser annealing. (c) The dynamic  $R_{on}$  versus  $V_{DSQ}$  for comparison. The inset shows the waveform of a pulsed  $I$ - $V$  measurement.

increased from  $1.74$  to  $2.96 \text{ m}\Omega\text{-cm}^2$  for the Si-implanted S/D HEMT, but increased from  $2.18$  to  $4.5 \text{ m}\Omega\text{-cm}^2$  for the reference sample. The result implies that better thermal stability was shown in the non-alloyed ohmic contact of HEMT. Figure 8(b) shows the  $I_{DS}$ - $V_{DS}$  curves under  $200^\circ\text{C}$  measurement, and the on-state resistance under high temperature measurement could be summarized in figure 8(c).

In the meantime, it is worth discussing the switching characteristics after pulsed laser annealing. The nitrogen vacancy ( $V_N$ ) generally acts as a surface trapping center, and is well known as the origin of the current collapse phenomenon [17]. The nitrogen vacancy and coordinate surface defect on the GaN surface is attributed to process injury, such as plasma-induced damage and thermal damage, which plays the role of the fixed positive charge. The positive charge at the surface trap will result in an electric field at the interface between the gate metal and GaN surface, and further induce serious gate leakage current regarding electron tunneling [17, 18]. Mechanisms of the reduction in gate leakage current by means of treatments have already been reported in previous discussions [19–23]. The surface treatment process is expected to remove the defects and impurities on the GaN surface. However, we can compare the gate leakage improvement after laser annealing. As shown in figure 9, the pulsed laser annealing leads to a remarkable reduction in gate leakage current under reverse bias. It means that we can improve the surface trap density via laser annealing. In contrast, the higher gate leakage of the reference sample implies that the nitrogen vacancy was formed and also induced surface defects due to high temperature annealing, which increased the Ga/N ratio of the GaN surface below the gate region. The RMS roughness of GaN was increased from  $1.1 \text{ nm}$  to  $3.5 \text{ nm}$  and is a clear evidence for this fact.

It could be summarized that the contact resistance and device performance depend on the implanted S/D technology characterized through DC measurement. The ion implantation, followed by pulsed laser annealing, was attributed to reduce the barrier thickness of S/D contacts. According to the TLM results, power density of pulsed laser annealing was responsible for the Si doping concentration of  $n$ -GaN for the S/D regions. Higher doping concentration of  $n$ -GaN will lead

to a sharp barrier of  $n$ -GaN, promising electron tunnelling through a thinner barrier. Therefore, the device performance and contact resistance show remarkable improvement. The significant reduction of the contact resistance also leads to a lower on-resistance. The on-resistance for a HEMT includes contact resistance ( $R_c$ ), resistance from source to gate ( $R_{sg}$ ), channel resistance ( $R_{ch}$ ), and resistance from drain to gate ( $R_{dg}$ ) [8]. In our case, we even add an extra resistance from implanted  $n$ -GaN ( $R_{imp}$ ), but the intensive reduction of contact resistance will result in a relatively lower on-state resistance.

In addition, the surface traps are also responsible for the current collapse phenomenon [17]. The on-state resistance was increased with increasing drain voltage. However, dispersion of the drain current or increased dynamic on-state resistance is a critical issue, which is required to be solved for power-switching applications. As shown in figures 10(a) and (b), the current collapse phenomena were induced by drain stress. Pulsed  $I_{DS}$ - $V_{DS}$  characteristics were extracted from the off-state with a quiescent gate bias ( $V_{GSQ}$ ) of  $-5 \text{ V}$  to the on-state at  $1 \text{ V}$  in  $500 \text{ ns}$  and a separation of  $1 \text{ ms}$ . The quiescent drain bias ( $V_{DSQ}$ ) was swept from  $0 \text{ V}$  to  $40 \text{ V}$  ( $10 \text{ V}$  step). As a result, this shows a smaller dispersion between  $V_{DSQ} = 0$  to  $40 \text{ V}$  after pulsed laser annealing, thereby the surface trap density was successfully decreased. The dynamic on-state resistance was investigated from the slope of the  $I_{DS}$ - $V_{DS}$  curve at different  $V_{DSQ}$ . Figure 10(c) summarized the dynamic  $R_{on}$  with varying  $V_{DSQ}$ , which shows a smaller discrepancy after pulsed laser annealing. The result also shows a consistent static on-state resistance under high temperature measurement. This result implies that the more stable  $R_{on}$  can be attributed to the eliminated surface trap states.

Therefore, we can conclude that the improvement of DC characteristics was ascribed to the remarkable reduction of S/D series resistance, and also corresponds to the reduction of surface trap density. Our ion-implantation technique and pulsed laser annealing not only solves the problem of a rough surface due to metal diffusion but also produces lower contact resistance for the HEMTs. Furthermore, better thermal stability and lower gate leakage was also obtained due to the

treatment by pulsed laser annealing, leading to reliable HEMTs with good switching ability.

## 5. Conclusion

We have demonstrated Si implantation incorporation into GaN HEMTs by using a non-alloyed ohmic contact process. The optimized power density of pulsed laser annealing successfully activates the implanted Si dopants, instead of using a general high temperature process. The experimental results show the GaN surface reformation under the high power density of the illumination conditions. It provides a good surface for the following contact engineering. It shows comparable contact resistance, and even demonstrates lower contact resistance to  $6.8 \times 10^{-7} \Omega \cdot \text{cm}^2$ . DC measurement of HEMTs shows better on-resistance, which was decreased from 2.18 to 1.74  $\text{m}\Omega\text{-cm}^2$  as we produced a lower contact resistance. Furthermore, pulsed laser annealing successfully improves the density of the surface trap, leading to a remarkable reduction of gate leakage. The pulse  $I$ - $V$  measurements also show a smaller dispersion after pulsed laser annealing, thereby the surface trap density was successfully decreased. Our results show the potential to increase yield, reproducibility, and reliability of GaN HEMTs. We also demonstrate the capability to integrate the GaN HEMT process into the present IC industry.

## Acknowledgements

This work was funded by the Ministry of Science and Technology of Republic of China under grant number, MOST 104-3113-E-009-002-CC2.

## References

- [1] Mitova R *et al* 2015 *IEEE Trans. Power Electron.* **29** 2441–52
- [2] Lu B *et al* 2010 *IEEE Electron Dev. Lett.* **31** 951–3
- [3] Lin M E *et al* 1994 *Appl. Phys. Lett.* **64** 1003–5
- [4] Dora Y *et al* 2006 *IEEE Electron Dev. Lett.* **27** 529–31
- [5] Lian Y W *et al* 2015 *IEEE Trans. Electron Dev.* **62** 519–24
- [6] Yu H *et al* 2005 *IEEE Electron Dev. Lett.* **26** 283–5
- [7] Recht F *et al* 2006 *IEEE Electron Dev. Lett.* **27** 205–7
- [8] Nomoto K *et al* 2007 *IEEE Electron Dev. Lett.* **28** 939–41
- [9] Porowski S *et al* 2003 *Proc. 5th Int. Conf. Nitride Semiconductors* p 70
- [10] Suski T *et al* 1999 *Mater. Sci. Eng. B* **59** 1–5
- [11] Dupuis R D *et al* 1999 *J. Electronic Mater.* **28** 319–24
- [12] Muth J F *et al* 1997 *Appl. Phys. Lett.* **71** 2572–4
- [13] Lu C *et al* 2002 *J. Appl. Phys.* **91** 9218–24
- [14] Lin Y J *et al* 2004 *J. Appl. Phys.* **95** 571–5
- [15] Chiu Y S *et al* 2014 *J. Vac. Sci. Technol. B* **32** 011216
- [16] Mohammed F M *et al* 2007 *J. Appl. Phys.* **101** 033708
- [17] Kotani J *et al* 2004 *J. Vac. Sci. Technol. B* **22** 2179–89
- [18] Saito W *et al* 2005 *IEEE Trans. Electron Dev.* **52** 159–64
- [19] Chen Z T *et al* 2011 *Appl. Phys. Lett.* **99** 183504
- [20] Romero M F *et al* 2012 *IEEE Trans. Electron Dev.* **59** 374–9
- [21] Chung J W *et al* 2008 *IEEE Electron Dev. Lett.* **29** 1196–8
- [22] Linkohr S *et al* 2012 *Phys. Status Solid c* **9** 1096–8
- [23] Vanko G *et al* 2009 *Vacuum* **84** 235–7